THE JOURNAL OF PHYSICAL CHEMISTRY A

Article

The Dynamics of Isolated 1,8-Naphthalimide and N-Methyl-1,8-Naphthalimide: An Experimental and Computational Study

Thiemo Gerbich, Hans-Christian Schmitt, Ingo Fischer, Roland Mitric, and Jens Petersen

J. Phys. Chem. A, **Just Accepted Manuscript** • DOI: 10.1021/acs.jpca.6b01226 • Publication Date (Web): 13 Mar 2016

Revised version, submitted J. Phys. Chem. A, March 10th, 2016

The Dynamics of Isolated 1,8-Naphthalimide and N-Methyl-1,8-Naphthalimide: An Experimental and Computational Study

Thiemo Gerbich, Hans-Christian Schmitt, Ingo Fischer, Roland Mitrić and Jens Petersen**

Institute of Physical and Theoretical Chemistry, University of Würzburg, Am Hubland, D-97074 Würzburg, Germany

AUTHOR INFORMATION

Corresponding Authors

ingo.fischer@uni-wuerzburg.de, phone: +49-931/31-86362

jens.petersen@uni-wuerzburg.de, phone: +49-931/31-88832

ABSTRACT

In this work we investigate the excited state structure and dynamics of the two molecules 1,8-naphthalimide (NI) and N-methyl-1,8-naphthalimide (Me-NI) in the gas phase by picosecond time- and frequency-resolved multiphoton ionization spectroscopy. The energies of several electronically excited singlet and triplet states and the S_1 vibrational wavenumbers were calculated. Nonadiabatic dynamics simulations support the analysis of the radiationless deactivation processes. The origin of the $S_1 \leftarrow S_0$ ($\pi\pi^*$) transition was found at 30 082 cm^{-1} for NI and at 29 920 cm^{-1} for Me-NI. Furthermore, a couple of low-lying vibrational bands were resolved in the spectra of both molecules. In the time-resolved scans a bi-exponential decay was apparent for both Me-NI and NI. The fast time constant is in the range of 10 – 20 ps, while the second one is in the nanosecond range. In accordance with the dynamics simulations, intersystem crossing to the fourth triplet state S_1 ($\pi\pi^*$) $\rightarrow$ T_4 ($n\pi^*$) is the main deactivation process for Me-NI due to a large spin-orbit coupling between these states. Only for significant excitation internal conversion via a conical intersection becomes a relevant deactivation pathway.

INTRODUCTION

The excited-state dynamics of several photoexcited heterocycles seems to be characterized by a competition between intersystem crossing (ISC) and internal conversion (IC) occurring on a picosecond time scale, as shown in previous studies on 9-fluorenone[1,2] and 1,8-naphthalic anhydride (NDCA).[3] Furthermore, in isolated NDCA the deactivation rate shows a strong dependence of the vibrational excess energy[3], which can be explained by a barrier separating the energy minimum of the lowest excited singlet state from a conical intersection (CI) to the ground state. Since the details of the electronic structure seem to influence the competition between IC and ISC, we extended our investigation to isolated 1,8-naphthalimide (NI) and N-methyl-1,8-naphthalimide (Me-NI), depicted in Scheme 1. In both molecules the electronic structure is altered by replacing one oxygen atom of NDCA by a nitrogen atom.

Scheme 1. Structure of a) NI (C_{2v} Symmetry) and b) Me-NI (C_s Symmetry). The coordinate axes used for determining the symmetry are shown in grey. The primarily planar molecules are orientated in the y-z plane.

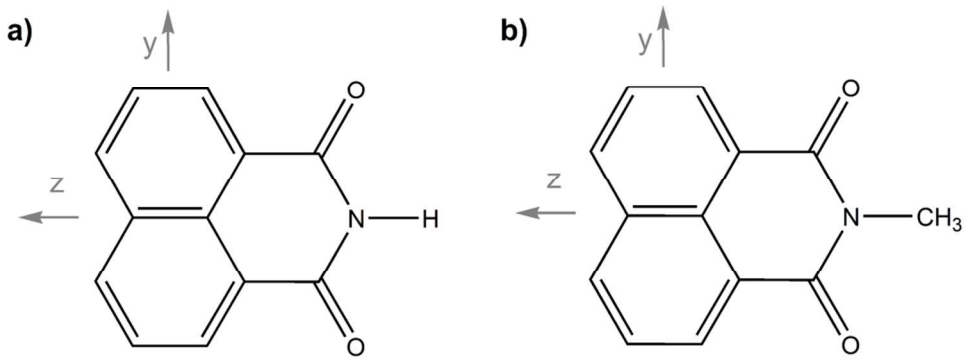

A second motivation for understanding the dynamics of radiationless deactivation after photoexcitation in these molecules is their relevance to energy and electron transfer in organic

materials.[4] Heterocycles like 1,8-naphthalimide (NI) and its derivatives show interesting optoelectronic properties and are used in a variety of applications, such as dyes, liquid crystal displays and in organic light emitting diodes.[5-7]

Until now no gas phase experiments of isolated naphthalimides have been reported. Nevertheless, these molecules have been of interest in a couple of previous studies. UV/Vis absorption spectra of several substituted NIs in solution have been reported.[8] The photophysical properties of NI and Me-NI in solution were examined by Wintgens et al.[9] For both molecules high quantum yields for intersystem crossing and short fluorescence lifetimes of $\tau < 130$ ps were found in nonpolar solvents. However, the ISC quantum yield decreases for more polar solvents, and fluorescence lifetimes in the nanosecond range were observed.[9] Computational studies of NI investigated the influence of solvent on absorption and fluorescence spectra and elucidated charge transfer processes of NI in different solvents.[10,11] The photophysical properties and charge transfer processes in more complex derivatives of NI have been addressed in further studies as well.[12-14]

To gain insight into the photophysical changes that occur upon replacing O by N, we investigated the excited state dynamics of isolated NI and Me-NI in a free jet by time-resolved photoionization and compare it to previous studies on NDCA. Me-NI was studied in addition to NI, because (a) due to its higher vapour pressure signals are larger and (b) neither tautomers nor hydrogen-bonded clusters that potentially perturb the spectra are expected to be present in the jet. The experiments are supported by time-dependent density functional theory (TDDFT) calculations to provide energies of low-lying electronically excited singlet and triplet states. Additionally, to study the coupled electron-nuclear dynamics and to interpret the deactivation processes, surface hopping simulations were carried out.

EXPERIMENTAL SECTION

Me-NI (m = 211 amu) was synthesized in one step from 1,8-naphthalic anhydride (NDCA) and methylamine ($MeNH_2$, 25 % aqueous solution) with a yield of nearly 100 %. The synthesis followed the route of Nicholson et al.[15] In contrast, NI and NDCA were obtained commercially from Sigma-Aldrich and used without further purification. While NI has a high melting point of approximately 300 °C,[16] for Me-NI a lower value of about 205 °C has been reported.[17] The gas phase experiments were carried out by heating the samples in a home-build oven attached to a pulsed solenoid valve. The molecules were heated up to 200 - 220 °C in an argon atmosphere (p_0(Ar) = 1.4 – 2.0 atm) and were expanded through a 1.0 mm diameter nozzle into a differentially pumped vacuum chamber. The detailed experimental setup has been described in a previous publication.[18]

For excitation and ionization of the supersonically cooled molecules picosecond pulses provided from a 10 Hz laser system introduced in ref. [19] were used. The system operates at a fundamental wavelength of 1053 nm delivered by a solid state Nd:YLF (neodymium-doped yttrium lithium fluoride) laser. In an optical parametric generator (OPG) 85 % of the third harmonic (7-8 mJ) was employed to generate tunable pump pulses with wavelengths in the range of 280 to 350 nm and pulse energies of 30 – 100 μJ. The residual part of the third harmonic with 200 – 300 μJ was sent over a motorized linear translation stage and subsequently used as the probe pulse. The bandwidth of the pulses was on the order of 20 cm^{-1} and the instrument response function (IRF) was found to be around 5 ps. The pump and probe pulses were overlapped on a dichroic mirror and slightly focused into the molecular jet. After acceleration of the molecular ions in a TOF mass spectrometer the ion signal was recorded on a multichannel plate detector. The data was

averaged for 75 – 100 shots per point for every scan and up to 12 scans were averaged to optimize the SNR.

COMPUTATIONAL SECTION

The structures of Me-NI and NI have been optimized in the framework of density functional theory (DFT) employing the CAM-B3LYP functional[20,21] combined with the def2-TZVP basis set,[22] and the energy minima have been confirmed by calculating the vibrational frequencies. Subsequently, the vertical electronic absorption spectra have been calculated using time-dependent density functional theory (TDDFT) employing the same functional and basis set. In order to determine the origin of the vibronic spectra between the electronic ground state and the lowest electronically excited state, the structures have been also optimized in the excited state, and the vibrational frequencies have been determined. All DFT calculations have been performed using the Gaussian 09 program package.[23]

The coupling between singlet and triplet states has been investigated by calculating spin-orbit matrix elements for selected DFT-optimized geometries of Me-NI. The spin-orbit coupling has been calculated using the Molpro program package,[24] employing the multi-reference configuration interaction method (MR-CI)[25-27] with reference configurations taken from a complete active space self-consistent field (CASSCF)[28] calculation. For this purpose, the 6-31G basis set has been employed, and the active space consisted of 12 electrons in 7 orbitals, while for the MRCI all single and double excitations from the active orbitals to higher virtual orbitals were taken into account.

The nonadiabatic relaxation from the first excited singlet state to the electronic ground state of Me-NI was investigated by employing Tully's surface hopping method[29]. To this end, a total

number of 100 initial nuclear coordinates and momenta were sampled from 30 ps long trajectories employing the semiempirical OM3 method[30] in the electronic ground state at 30 K or 300 K, respectively. Subsequently the nonadiabatic dynamics was performed using the OM3 method[30] combined with MR-CI[31,32] in the framework of the MNDO program,[33]. The active space consisted of 14 electrons in 11 orbitals, and all single and double excitations out of the ground state SCF and the HOMO-LUMO excited configuration were taken into account.[31-33] The nuclear motion was simulated by numerically solving Newton's equations of motion with a time step of 0.2 fs using the velocity Verlet algorithm.[34] The electronic state coefficients needed for determining the hopping probabilities between electronic states were calculated along each trajectory by numerical integration of the time-dependent Schrödinger equation including the nonadiabatic coupling.

Similarly, also nonadiabatic dynamics simulations within the four lowest triplet states were performed employing the same set of 100 initial conditions as for the singlet state dynamics. As the initial state, the T_4 state was chosen, which lies energetically close to the first excited singlet state. These simulations served to determine the order of magnitude of the nonadiabatic couplings within the triplet state manifold. For this purpose, a propagation time of 100 fs, during which population transfer from the T_4 to all of the lower-lying states occurred, was sufficient to obtain average values for the nonadiabatic coupling elements (see below).

In addition to the nonadiabatic dynamics in the singlet states, the electronic state population dynamics in the full manifold of two singlet and four triplet states has been simulated on a model level. For this purpose, the time-dependent Schrödinger equation

$$i\hbar\dot{c}_i = E_i c_i - \sum_j \left(i\hbar D_{ij} - H_{ij}^{SO}\right) c_j \qquad (1)$$

including the electronic energies E_i, the nonadiabatic couplings D_{ij} and the spin-orbit couplings H_{ij}^{SO} has been integrated numerically over a time duration of 50 ps. The energies and spin-orbit couplings have been initially assigned the values obtained for the S_1 state minimum structure. The nonadiabatic couplings have been averaged from surface-hopping simulations in the singlet and triplet manifolds as described above. Additionally, in order to mimic the fluctuations of energies and couplings due to nuclear motion, the initial values have been modified in each time step by a random term, which for the energies could assume a value up to 0.05 eV, while for the couplings a variation up to the size of the initial coupling was made possible. In this way, time-dependent populations of all involved singlet and triplet states have been obtained.

RESULTS

The vertical excitation energies of the lowest singlet and triplet states of NI and Me-NI calculated by TDDFT are summarized in Table 1. For comparison the excitation energies of NDCA from ref. [3] are listed as well. While the C_{2v} symmetric NI is planar (like NDCA), Me-NI shows only C_s symmetry due to the non-planarity of the methyl group. Nevertheless the excitation energies to the first excited states are very similar for NI and Me-NI. For both molecules the lowest excited singlet state is accessible upon near-UV excitation and bears a high oscillator strength. The second excited singlet state is located 0.23 eV above the S_1 for Me-NI and 0.24 eV above for NI. The calculated adiabatic energy differences between the vibronic origins of S_1 and S_2 even amount to 0.42 eV in both cases. Therefore, electronic coupling between these states can most likely be neglected.

Close to or below the ($\pi\pi^*$) S_1 state several triplet states are located, at least one of them with $n\pi^*$ character. According to the El-Sayed rules[35] significant spin orbit coupling and thus considerable intersystem crossing rates can be expected between states of $n\pi^*$ and $\pi\pi^*$ character.

Table 1: Vertical excitation energies of the low-lying electronic states of isolated Me-NI, NI and NDCA at the S_0 minimum geometry, determined by TDDFT calculations.

Vertical excitation energies /eV								
Me-NI			**NI**			**NDCA** (Ref. [3])		
T_1	$^3A'$ ($\pi\pi^*$)	2.32	T_1	$^3A_1$ ($\pi\pi^*$)	2.32	T_1	$^3A_1$ ($\pi\pi^*$)	2.32
T_2	$^3A'$ ($\pi\pi^*$)	3.57	T_2	$^3B_2$ ($\pi\pi^*$)	3.56	T_2	$^3B_2$ ($\pi\pi^*$)	3.55
T_3	$^3A'$ ($\pi\pi^*$)	3.87	T_3	$^3B_2$ ($\pi\pi^*$)	3.86	T_3	$^3B_2$ ($\pi\pi^*$)	3.83
T_4	$^3A''$ ($n\pi^*$)	4.00	T_4	$^3B_1$ ($n\pi^*$)	4.01	S_1	$^1A_1$ ($\pi\pi^*$)	4.17
S_1	$^1A'$ ($\pi\pi^*$)	4.13	S_1	$^1A_1$ ($\pi\pi^*$)	4.14	T_4	$^3B_1$ ($n\pi^*$)	4.21
T_5	$^3A''$ ($n\pi^*$)	4.23	S_2	$^1B_2$ ($\pi\pi^*$)	4.38	S_2	$^1B_2$ ($\pi\pi^*$)	4.40
S_2	$^1A'$ ($\pi\pi^*$)	4.36	S_3	$^1B_1$ ($n\pi^*$)	4.39	S_3	$^1B_1$ ($n\pi^*$)	4.63

N-Methyl-1,8-Naphthalimide

The one-color photoionization mass spectrum of Me-NI recorded at 314 nm excitation is depicted in the upper trace of Figure 1. The molecular signal at m/z = 211 shows the highest intensity in the spectrum and is accompanied by a couple of fragments. The signals at m/z = 183 and m/z = 167 originate from a loss of CO or CO_2, respectively. The smaller fragments at m/z = 154 and m/z = 126 were generated by dissociation of the (-N-Me) group and are equivalent to the fragments found in mass spectra of NI, recorded at 332 nm (lower trace), or NDCA.[3] All

fragments originate from dissociative photoionization because the recorded REMPI spectra are similar in all mass channels.

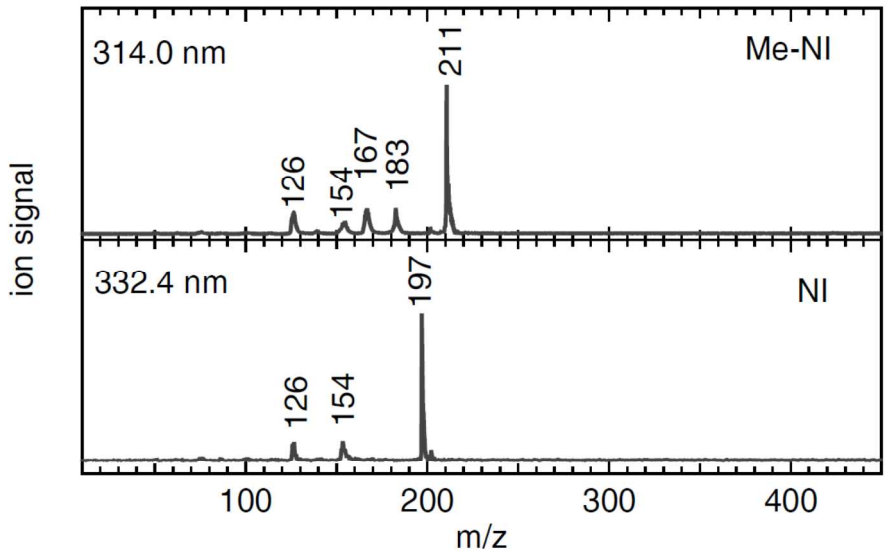

Figure 1. Mass spectrum of Me-NI (top graph) and NI (bottom graph) recorded at 314 nm and 332.4 nm respectively. The peak at m/z=211 is due to Me-NI ion, while the peak at m/z = 197 corresponds to NI.

The vertical ionization energy of Me-NI was determined by photoelectron spectroscopy to be 8.57 eV.[36] Therefore two 351 nm (3.53 eV) photons are necessary for ionization from the S_1 state. By scanning the excitation laser from 320 nm to 340 nm a [1+2'] REMPI spectrum was recorded. The first band in the spectrum shown in Figure 2 was found at 29 920 cm^{-1} and is assigned to the origin of the S_1 state. Furthermore three distinct peaks are observed at +208 cm^{-1}, +308 cm^{-1} and +418 cm^{-1} and represent S_1 vibrationally excited states. With higher excitation energies the background signal increases, probably due to the large density of vibronic states, and prohibits an assignment of further bands in the Me-NI spectrum. The small shoulder at the beginning of the spectrum around 29 700 cm^{-1} is due to hot band or sequence band transitions.

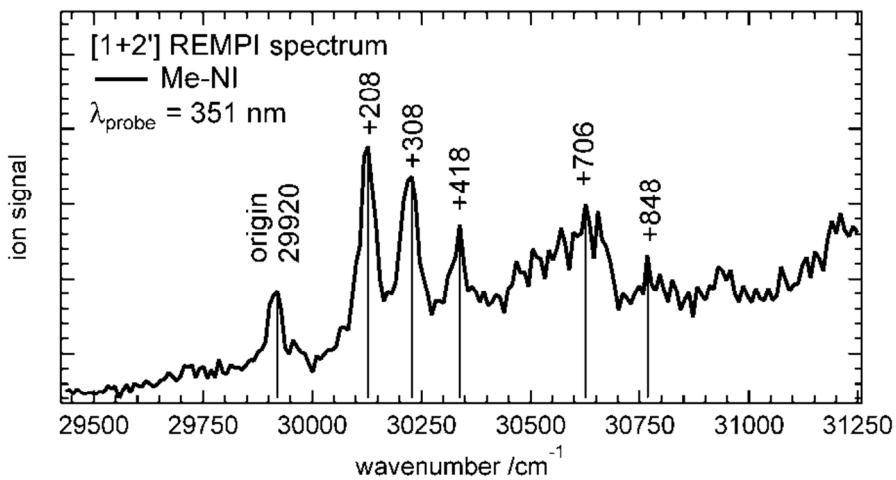

Figure 2. The two-color REMPI spectrum of isolated Me-NI recorded at t_0. The peak at 29 920 cm^{-1} is assigned to the band origin of the $S_1 \leftarrow S_0$ transition.

Employing TDDFT, the origin of the vibronic excitation spectrum was computed at an energy of 3.735 eV (30 120 cm^{-1}), which agrees within 25 meV with the experimentally determined value of 3.710 eV (29 920 cm^{-1}). The difference of 0.4 eV compared to the vertical excitation energy given in Table 1 indicates a slight geometry change upon excitation.

In Table 2 the experimentally observed vibrational bands are compared to the values computed by TDDFT calculations. The majority of the bands is assigned to totally symmetric bending modes of the molecule. Even in case of a free torsion of the N-Me-group, which would lead to a C_{2v} symmetry instead of the originally assumed C_S symmetry, these bands represent allowed transitions into A_1 bands. Due to the similar minimum energy structure of S_1 and S_0, Franck-Condon factors for non-totally symmetric transitions will be small.

Table 2. Comparison of experimental and calculated wavenumbers for the vibrational bands of the S_1 state of Me-NI.

rel. wavenumber /cm^{-1}	λ_{exc} /nm	calc. vibrational transition /cm^{-1}	assignment
29 920	334.2	30 120	0_0^0
+208		+271	46 A’
+308		+363	45 A’
+418	329.6	+419 / +454	42 A’ / 41 A’/ (46 A’)^2
+547		+567	39 A’
+650		+635	38 A’
+706	326.5	+695 / +731	37 A’ / (12 A’’)^2
+848		+821	36 A‘

In the next step time-resolved pump-probe spectra were measured for most of the vibronic bands summarized in Table 2. In Figure 3 three exemplary delay scans at different excitation energies are depicted. In all scans the temporal decay is fitted by a biexponential function. The second time constant τ_2 exceeds the time-scale of the experiment and was considered in the fit function with a fixed time constant of 1 ns. For the S_1 origin a fast decay of τ_1= (14.1±1.4) ps was observed (top graph of Figure 3). Other vibronic bands of the S_1 state with higher excitation energies yielded similar lifetimes in the range between 12 and 16 ps and show a similar long-lived offset.

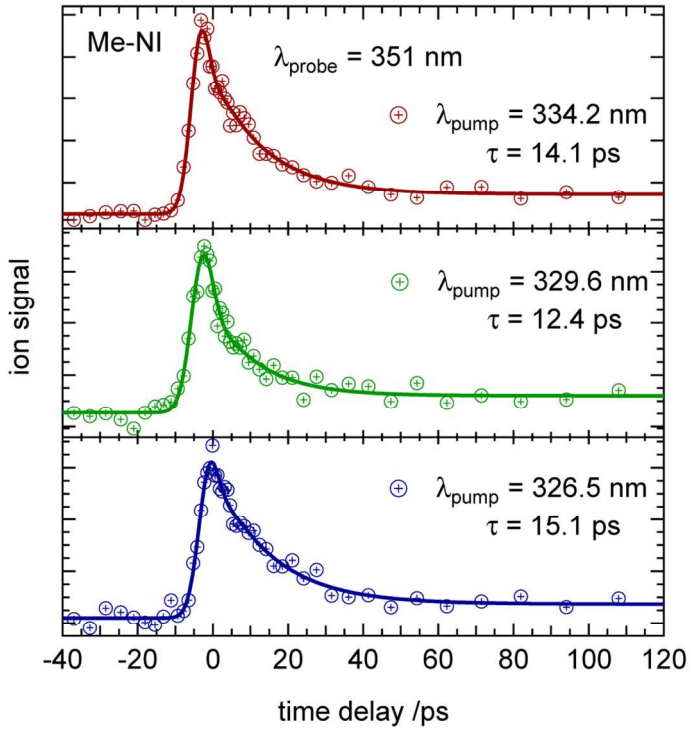

Figure 3. Selected delay scans of Me-NI with different excitation energies. In every scan a two-step deactivation is observed with a fast time constant of 12-16 ps and a second, much slower process.

1,8-Naphthalimide

In addition to Me-NI we investigated the chemically similar molecule NI (see Scheme 1). Its vertical ionization energy was determined to be 8.68 eV, slightly higher compared to Me-NI.[36] Again two probe photons are required for ionization from the S_1 state. The mass spectrum of NI (m/z = 197), given in the lower trace of Figure 1 and recorded at 332.4 nm, also shows fragments at m/z = 154 and m/z = 126 resulting from CO/NH- and 2× CO/NH-loss, respectively, due to dissociative photoionization. Unlike the cases of Me-NI and NDCA, there are no signals resulting from CO- or CO_2-loss. Note that no dimer signal is present. Cluster formation has been suppressed in the experiments by recording spectra early in the jet. Using the same delay between

laser and pulsed valve as in the experiments on Me-NI, a substantial amount of dimers and higher clusters was observed.

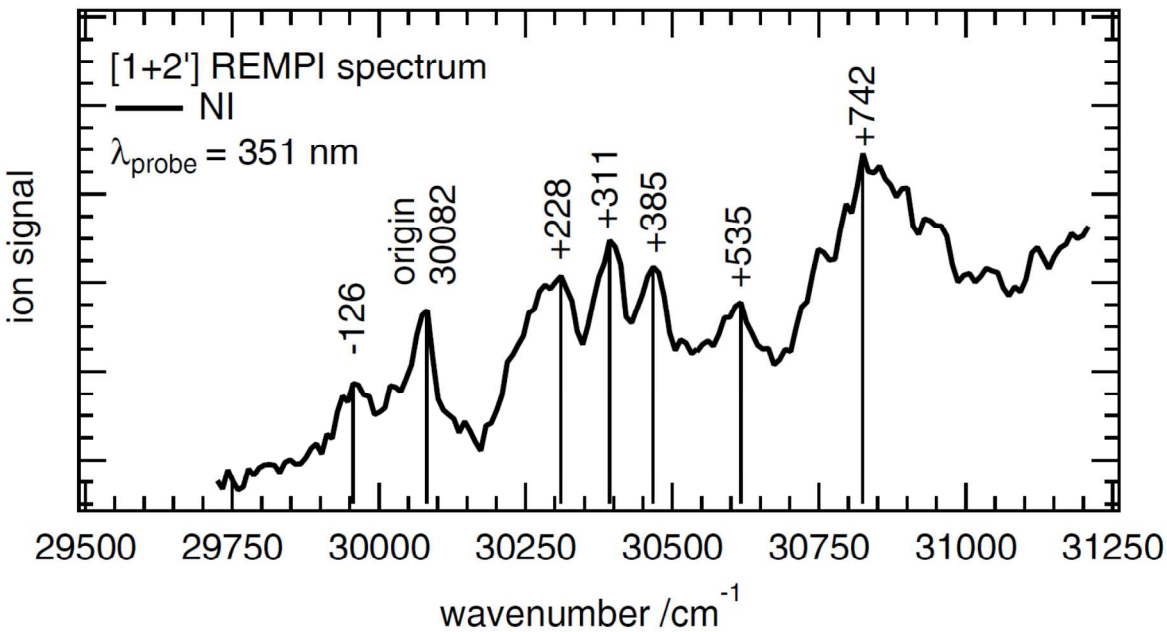

Figure 4. The two-color REMPI spectrum of isolated NI at t_0. The peak at 30082 cm^{-1} is assigned to the origin of the $S_1 \leftarrow S_0$ transition.

The first excited state was also investigated by a [1+2'] REMPI. The pump-pulses were tuned between 320 and 336 nm and the third harmonic of the Nd:YLF laser was again used for ionization, the resulting spectrum is depicted in Figure 4. Like in Me-NI, the background signal increases with higher excitation energies due to the increasing density of states. Two peaks 126 cm^{-1} apart appear around 30000 cm^{-1}. It is tempting to assign the first peak at 29 956 cm^{-1} to the S_1 origin, because a shift of +36 cm^{-1} for methyl-substitution appears reasonable. Two factors conflict with this assignment: First, a band at +126 cm^{-1} does not match the computed value of any totally symmetric vibration. Second, there is a pattern of three close-lying vibronic bands that also appears in the spectra of Me-NI and NDCA. Values of +354 cm^{-1}, +437 cm^{-1} and +511 cm^{-1} would correspond to significantly higher vibrational energies than in the related molecules.

Choosing the band at 30082 cm^{-1} as the origin leads to vibrational bands at +228 cm^{-1}, +311 cm^{-1} and +385 cm^{-1}. Further bands then appear +535 cm^{-1} and 742 cm^{-1}. The vibrational spacings are then very similar for NI and Me-NI, as we would expect for such similar molecules. We therefore prefer the latter assignment. Based on TDDFT calculations nearly all appearing bands can be attributed to in-plane bending modes of A_1 symmetry. A summary of all observed vibronic bands and their assignment is given in Table 3. Only the lowest energy band at +228 cm^{-1} is assigned to the first overtone of a B_1 vibration. Such a band was also visible in NDCA and has also been assigned to a B_1 overtone[3].The right-hand column in Table 3 lists observed bands in NDCA for comparison. As expected the observed spacings are similar to those in Me-NI summarised in Table 2.

Consequently, we have to discuss the assignment of the band at 29 956 cm^{-1}, red-shifted by -126 cm^{-1}. There are three possible reasons for this band, none of them fully convincing. First it might be assigned to the lactim tautomer of NI. In fact, a transition energy of 29097 cm^{-1} was computed for the origin of its $S_2 \leftarrow S_0$ vibronic excitation spectrum. Since the lactim tautomer lies roughly 80 $kJ{\cdot}mol^{-1}$ above the lactam, significant population in a free jet is rather improbable. Second, the band might originate from a cluster fragment. In the mass spectrum (cf. lower trace Figure 1) no cluster signals are visible, so we would have to assume a complete fragmentation of the cluster. However, the wavenumber shift is in the range that could be expected for the cluster with one water molecule. Due to the significant geometry change upon ionization this cluster might ohotoionize dissociatively. Finally the band might be assigned to a hot- or sequence band. In order to avoid cluster formation we chose comparably warm conditions in the jet that might lead to insufficient cooling of low-frequency modes. This is evidenced in the spectrum by the broader

bands in comparison to Me-NI. Nevertheless the band would be unusually intense for a hot or sequence band.

Table 3. Experimental and computed wavenumbers for the vibrational bands of the S_1 State of NI.

rel. wavenumber /cm^{-1}	λ_{exc} /nm	calc. vibrational transition /cm^{-1}	tentative assignment	observed band NDCA /cm^{-1}
-126				
30 082	332.4	30 252	0_0^0	
+228	329.9	+2·137	$(11\ B_1)^2$	+249
+311	329	+356	21 A_1	+366
+385		+440 / +465	20 A_1 / 19 A_1	+432
+535		+465 / +583	19 A_1 / 18 A_1	+555
+742		+698	17 A_1	+713

In order to study the dynamics of the first excited state we also performed ps-time-resolved pump-probe experiments. Several bands visible in Figure 4 were excited and their lifetimes were probed. Figure 5 shows some selected delay-traces. Like in Me-NI all bands show a fast time constant τ_1 between 10 to 17 ps and a long-lived signal, which is still present after 250 ps and indicates a second much slower decay. In isolated NI no systematic dependence of the lifetime on the excitation energy of the vibronic states can be found.

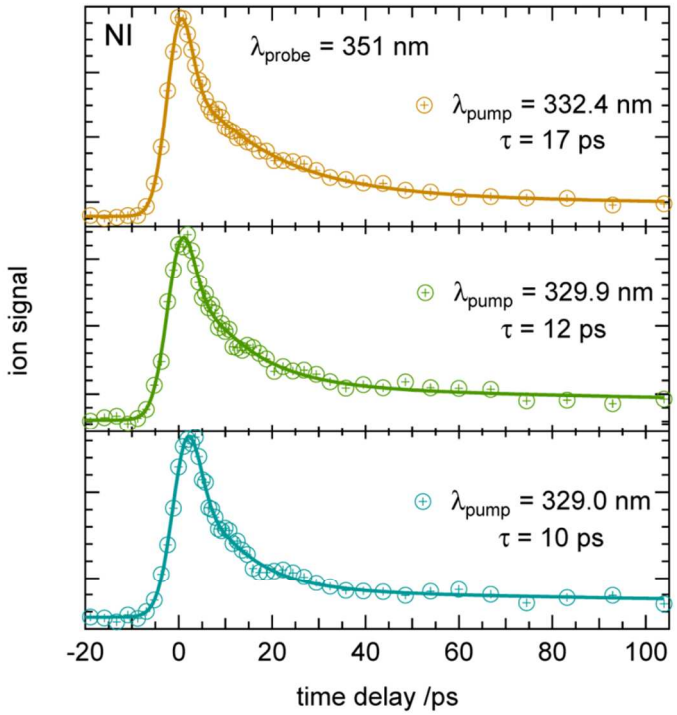

Figure 5. Selected time-delay traces of isolated NI. The pump wavelength is indicated in the figure. A two-step decay is assumed with short time constants of roughly 10 – 20 ps and a second, slower decay.

Surface Hopping Dynamics Simulations

To gain a mechanistic insight into the excited state deactivation pathways, molecular dynamics simulations were carried out for Me-NI. In a first step, the nonadiabatic relaxation within the singlet manifold was investigated by Tully's surface hopping method.

All molecules were initialized in the first excited singlet state. Two different temperatures (30 K and 300 K) were simulated by choosing different initial conditions of spatial coordinates and momenta. The resulting population dynamics of the S_1 and S_0 state is depicted in Figure 6.

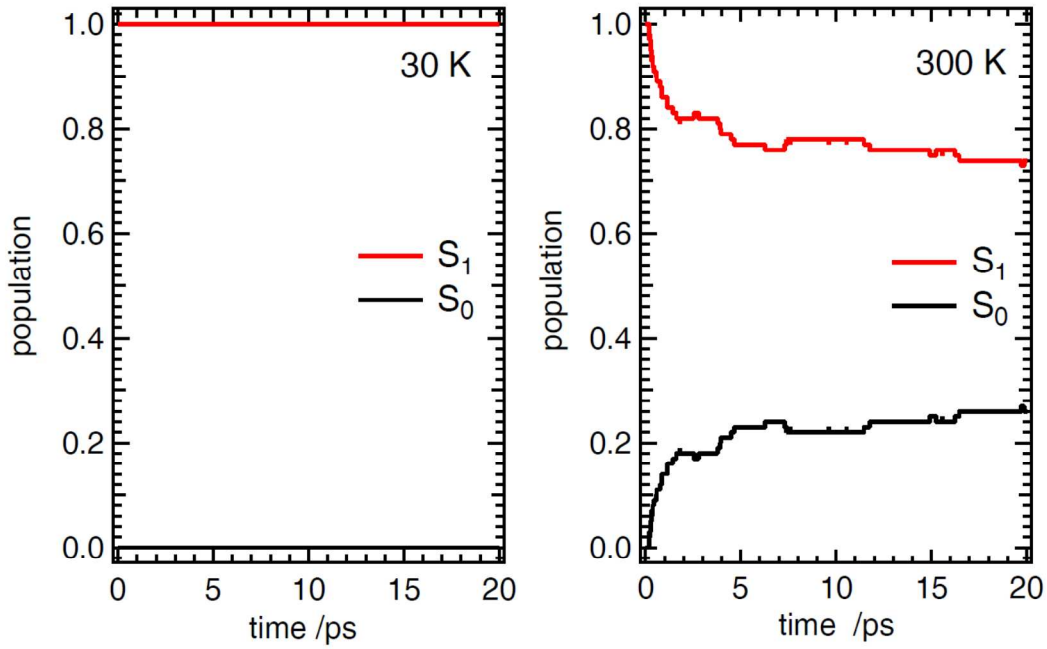

Figure 6. Evolution of the S_1 and S_0 population of Me-NI for 30 K and 300 K obtained from surface hopping dynamics.

In the case of cold molecules with a small amount of vibrational energy, corresponding to the conditions assumed in the free jet experiments, no population transfer into the ground state was found within 20 ps. Simulation with a temperature of 300 K yielded a partial deactivation of the S_1 state through a conical intersection (CI). The latter is characterized by the methyl group moving out of the ring plane as well as by a bond elongation between nitrogen and one of the neighboring carbonyl carbon atoms. However, 70 to 80 % of the population stays in S_1. This can be explained by an energy barrier on the S_1 surface that must be overcome by the molecules in order to reach the CI. The effective height of this barrier can be estimated from the dynamics simulations to be 0.5-0.6 eV. Far away from the CI the nonadiabatic coupling between the S_0 and the S_1 state is weak (approx. 6 cm^{-1}) and would only result in a slow deactivation via internal conversion. This is apparent from the simulation with cold molecules at 30 K shown in Figure 6.

In the second step the depopulation of the S_1 state of Me-NI via an intersystem crossing (ISC) to the triplet manifold is considered. The matrix elements for the spin orbit coupling between S_0, S_1 and the four lowest triplet states were calculated at the DFT-optimized S_1 geometry, as described above in the computational section. The resulting spin-orbit couplings are mostly negligible ($< 5\cdot10^{-2}$ cm^{-1}) except for the transition from the S_0 and S_1 states, which bear $\pi\pi^*$ character, to the fourth triplet state (^{3}A'' $n\pi^*$), with matrix elements of 46 and 15 cm^{-1}, respectively (for the values of all spin-orbit couplings employed in the simulation cf. Supporting Information (SI), Table S2). This is in accordance to the El-Sayed rules that predict an allowed electronic transition between $^1(\pi\pi^*)$ and $^3(n\pi^*)$ states.[35] Within the triplet manifold, nonadiabatic couplings with averaged values of 30-590 cm^{-1} were determined from surface-hopping calculations (cf. SI, Table S3), thus efficient IC processes populating the low-lying triplet states will take place after ISC from the S_1 to the T_4 state.

To investigate the coupled population dynamics including the two lowest singlet and four triplet states, an additional simulation was performed on a model level. For this purpose, the electronic energies obtained at the optimized S_1 geometry were employed (for the values cf. SI, Table S1), as well as the nonadiabatic and spin-orbit couplings alluded to above (cf. SI, Tables S2 and S3), and the time-dependent Schrödinger equation was integrated in this manifold of states as described in detail in the Computational section. Note that in the simulation a deactivation via a conical intersection is not included. The resulting population dynamics of Me-NI is shown in Figure 7, indicating a depopulation of the initially excited S_1 state on the ps-time scale.

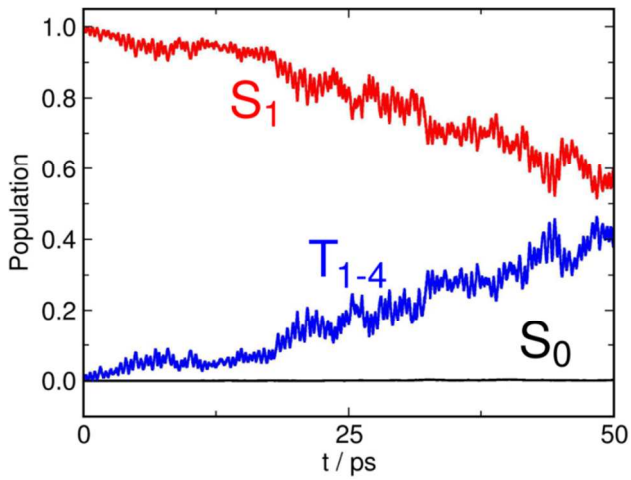

Figure 7. Calculated electronic relaxation dynamics of Me-NI involving singlet and triplet states. Population dynamics of the states S_0, S_1 and the sum of all four triplet states $T_{1\text{-}4}$ obtained by a model simulation employing the DFT energies for the optimized S_1 state geometry as well as nonadiabatic and spin-orbit couplings.

After 50 ps the population of the S_1 state has decreased to 55 % while the population of the triplet states $T_{1\text{-}4}$ has grown accordingly to 45 %. A significant population transfer to electronic ground state is not observed. The model confirms an effective deactivation to the triplet manifold due to ISC from the S_1 to the T_4 state. The corresponding time constant is in the order of 10-100 ps.

DISCUSSION

The results of the nonadiabatic dynamics simulations of Me-NI immediately lead to an interpretation of the two time constants observed in the experiment: The short time constant τ_1, which is on the order of 10 – 20 ps is assigned to ISC from the photoexcited S_1 ($\pi\pi^*$) state to the T_4 ($n\pi^*$), while τ_2, which is assumed to be > 500 ps corresponds to the lifetime of the T_1 ($\pi\pi^*$) state. Although the computed time constant is larger than the experimental one, the order of magnitude agrees. The intermediate internal conversion within the triplet manifold is very fast

and cannot be resolved within the time resolution of our experiment. The fast ISC can be explained by a large spin-orbit coupling in accordance with the El Sayed rules and the small energy gap. The T_4 state was computed to lie 0.13 eV (~ 1000 cm^{-1}) above the S_1 state. Given the accuracy of the computational methods the two states can be considered to be almost degenerate. According to Fermis golden rule[37] a high deactivation rate can be expected under these conditions. This interpretation is in accordance with transient absorption measurements of Me-NI in nonpolar solutions where the quantum yield Φ_{ISC} for a $S_1 \rightarrow T_x$ transition was determined to be close to 100 %.[9] Such fast ISC is not uncommon in carbonyl compounds. In benzophenone, for example, a time constant of 5 ps was found for the T_2 ($\pi\pi^*$)$\rightarrow S_1$ ($n\pi^*$) non-radiative transition.[38]

On the other hand the probability for IC within the singlet manifold is small at the temperature of a free jet (30 K). The surface hopping simulations show that a deactivation of the excited S_1 to the ground state via a conical intersection is only possible at high internal energies, because of a barrier on the excited state surface.

Although the dynamics was only simulated for Me-NI, a similar excited-state deactivation is assumed for NI, since the additional methyl group has little influence on the electronic structure and because similar results have been obtained in the experiments. The S_1 and T_4 states (see Table 1) are again almost degenerate, and ISC should be efficient in accordance with the El-Sayed rules. The deactivation of the S_1 state of NI is thus also attributed to ISC.

It is interesting to compare the dynamics of NI and Me-NI to the one of NDCA, which has an oxygen atom instead of the N-H or N-Me group and was investigated previously.[3] NDCA deactivates around the S_1 origin by ISC within roughly 1 ns, but IC increasingly dominates at higher vibronic excitation. In contrast, IC is not important for isolated Me-NI and NI at low temperatures. ISC is much faster and no significant dependence on the excess energy was found.

While the S_1/T_4 energy gap is similar in all three molecules, calculations yield a SOC matrix element of 15 cm^{-1} for Me-NI, somewhat larger than the value 10 – 11 cm^{-1} computed for NDCA. The average coupling element for $S_1 \rightarrow S_0$ internal conversion is on the other hand only slightly smaller in Me-NI compared to NDCA (6 cm^{-1} vs. 9 cm^{-1}). While for NDCA the simulations showed internal conversion to be efficient at 300 K, it remains incomplete in Me-NI. Interestingly the barrier to the S_1/S_0 conical intersection on the excited state surface is slightly smaller in Me-NI (0.6 eV compared to 0.7-0.9 eV in NDCA). It seems that access to the CI requires a larger degree of structural rearrangement in NI and Me-NI and thus ISC remains the dominant deactivation pathway even at significant internal excitation.

CONCLUSION

The dynamics of the S_1 state of isolated Me-NI and NI has been investigated by both picosecond laser spectroscopy and molecular dynamics simulations. The S_1 state origins were found at 29 920 cm^{-1} (3.710 eV) for Me-NI and 30 082 cm^{-1} (3.729 eV) in excellent agreement with TDDFT computations. In NI a further band appears at 29 956 cm^{-1} (3.714 eV), which might be assigned to the lactim tautomer, a cluster fragment or a hot or sequence band. The similar adiabatic excitation energies indicate a small influence of the methyl group on the electronic structure. The REMPI spectra show a few vibronic bands which appear at slightly different relative energies in the two molecules due to the presence of the N-methyl group. They can mostly be assigned to in-plane bending modes. A two-step deactivation was observed for both molecules. The first time constant, which is in the range of 10-20 ps for both molecules is assigned to a fast ISC into the T_4 ($n\pi^*$) state. ISC is followed by rapid internal conversion to the lowest triplet state. The second much slower time constant on the nanosecond range corresponds to photoionization from the lowest triplet state. In contrast to the related molecule NDCA

intersystem crossing remains the dominant deactivation pathway over the investigated energy range.

ASSOCIATED CONTENT

Supporting Information. Additional computational information (Electronic energies obtained at the optimized S_1 geometry, nonadiabatic and spin-orbit couplings) and full references 4 and 23. This material is available free of charge via the Internet at http://pubs.acs.org

ACKNOWLEDGMENT

The work was founded by the Deutsche Forschungsgemeinschaft within project FI 575/9-x. H.-C. S. acknowledges financial support by the "Fonds der Chemischen Industrie". We would like to thank Eileen Welz for her help in some of the experiments.

REFERENCES

(1) Gerbich, T.; Herterich, J.; Köhler, J.; Fischer, I. Time-Domain Study of the S_3 State of 9-Fluorenone. *J. Phys. Chem. A* **2014**, *118*, 1397-1402.

(2) Köhler, J.; Hemberger, P.; Fischer, I.; Piani, G.; Poisson, L. Ultrafast Dynamics of Isolated Fluorenone. *J. Phys. Chem. A* **2011**, *115*, 14249-14253.

(3) Gerbich, T.; Schmitt, H.-C.; Fischer, I.; Petersen, J.; Albert, J.; Mitric, R. Time-Resolved Study of 1,8-Naphthalic Anhydride and 1,4,5,8-Naphthalenetetracarboxylic Dianhydride. *J. Phys. Chem. A.* **2015**, *119*, 6006–6016.

(4) Alivisatos, P.; Barbara, P. F.; Castleman, A. W.; Chang, J.; Dixon, D. A.; Klein, M. L.; McLendon, G. L.; Miller, J. S.; Ratner, M. A.; Rossky, P. J. et al. From Molecules to Materials: Current Trends and Future Directions. *Adv. Mater.* **1998**, *10*, 1297-1336.

(5) Stewart, W. W. Functional Connections between Cells as Revealed by Dye-Coupling with a Highly Fluorescent Naphthalimide Tracer. *Cell* **1978**, *14*, 741-759.

(6) Grabchev, I.; Moneva, I.; Bojinov, V.; Guittonneau, S. Synthesis and Properties of Fluorescent 1,8-Naphthalimide Dyes for Application in Liquid Crystal Displays. *J. Mater. Chem.* **2000**, *10*, 1291-1296.

(7) Kolosov, D.; Adamovich, V.; Djurovich, P.; Thompson, M. E.; Adachi, C. 1,8-Naphthalimides in Phosphorescent Organic LEDs: The Interplay between Dopant, Exciplex, and Host Emission. *J. Am. Chem. Soc.* **2002**, *124*, 9945-9954.

(8) Alexiou, M. S.; Tychopoulos, V.; Ghorbanian, S.; Tyman, J. H. P.; Brown, R. G.; Brittain, P. I. The UV-Visible Absorption and Fluorescence of Some Substituted 1,8-Naphthalimides and Naphthalic Anhydrides. *J. Chem. Soc., Perkin Trans. 2* **1990**, 837-842.

(9) Wintgens, V.; Valat, P.; Kossanyi, J.; Biczok, L.; Demeter, A.; Berces, T. Spectroscopic Properties of Aromatic Dicarboximides. Part1.-N-H and N-Methyl-Substituted Naphthalimides. *J. Chem. Soc. Faraday Trans.* **1994**, *90*, 411-421.

(10) Jacquemin, D.; Perpète, E. A.; Scalmani, G.; Frisch, M. J.; Ciofini, I.; Adamo, C. Fluorescence of 1,8-Naphthalimide: A PCM-TD-DFT Investigation. *Chem. Phys. Lett.* **2007**, *448*, 3-6.

(11) Manna, A.; Chakravorti, S. Charge Transfer in 1,8-Naphthalimide: A Combined Theoretical and Experimental Approach. *Photochem. Photobiol.* **2010**, *86*, 47-54.

(12) Patsenker, L. D.; Artyukhova, Y. Y. Molecular Structure and Spectral Properties of Thionaphthalimides. *J. Mol. Struct.* **2003**, *655*, 311 - 320.

(13) Gan, J.; Chen, K.; Chang, C.-P.; Tian, H. Luminescent Properties and Photo-Induced Electron Transfer of Naphthalimides with Piperazine Substituent. *Dyes Pigm.* **2003**, *57*, 21 - 28.

(14) de Silva, A. P.; Goligher, A.; Gunaratne, H.; Rice, T. The pH-Dependent Fluorescence of Pyridylmethyl-4-Amino-1,8-Naphthalimides. *Arkivoc* **2003**, *7*, 229-243.

(15) Nicholson, B. K.; Crosby, P. M.; Maunsell, K. R.; Wyllie, M. J. An Orthomanganation Route to 2-Substituted Derivatives of N-Methyl-1,8-Naphthalimide. *J. Organomet. Chem.* **2012**, *716*, 49 - 54.

(16) Hargreaves, M. K.; Pritchard, J. G.; Dave, H. R. Cyclic Carboxylic Monoimides. *Chem. Rev.* **1970**, *70*, 439-469.

(17) Gompper, R. Uber den Verlauf der Methylierung von Carbonsaureamiden mit Diazomethan, II *Chem. Ber.* **1960**, *93*, 198-209.

(18) Schon, C.; Roth, W.; Fischer, I.; Pfister, J.; Kaiser, C.; Fink, R. F.; Engels, B. Paracyclophanes as Model Compounds for Strongly Interacting π-Systems. Part 1. Pseudo-Ortho-Dihydroxy[2.2]Paracyclophane. *Phys. Chem. Chem. Phys.* **2010**, *12*, 9339-9346.

(19) Auerswald, J.; Engels, B.; Fischer, I.; Gerbich, T.; Herterich, J.; Krueger, A.; Lang, M.; Schmitt, H.-C.; Schon, C.; Walter, C. The Electronic Structure of Pyracene: A Spectroscopic and Computational Study. *Phys. Chem. Chem. Phys.* **2013**, *15*, 8151-8161.

(20) Yanai, T.; Tew, D. P.; Handy, N. C. A New Hybrid Exchange-Correlation Functional Using the Coulomb-Attenuating Method (CAM-B3LYP). *Chem. Phys. Lett.* **2004**, *393*, 51 - 57.

(21) Berning, A.; Schweizer, M.; Werner, H.-J.; Knowles, P. J.; Palmieri, P. Spin-Orbit Matrix Elements for Internally Contracted Multireference Configuration Interaction Wavefunctions. *Mol. Phys.* **2000**, *98*, 1823-1833.

(22) Weigend, F.; Ahlrichs, R. Balanced Basis Sets of Split Valence, Triple Zeta Valence and Quadruple Zeta Valence Quality for H to Rn: Design and Assessment of Accuracy. *Phys. Chem. Chem. Phys.* **2005**, *7*, 3297-3305.

(23) Frisch, M. J.; Trucks, G. W.; Schlegel, H. B.; Scuseria, G. E.; Robb, M. A.; Cheeseman, J. R.; Scalmani, G.; Barone, V.; Mennucci, B.; Petersson, G. A. et al. *Gaussian 09 Revision A.02*, Gaussian Inc. Wallingford CT, 2009.

(24) Werner, H.-J.; Knowles, P. J.; Knizia, G.; Manby, F. R.; Schütz, M. *MOLPRO, Version 2012.1, a Package of Ab Initio Programs*, Cardiff University: Cardiff, UK, 2012.

(25) Knowles, P. J.; Werner, H.-J. An Efficient Method for the Evaluation of Coupling Coefficients in Configuration Interaction Calculations. *Chem. Phys. Lett.* **1988**, *145*, 514 - 522.

(26) Werner, H.-J.; Knowles, P. J. An Efficient Internally Contracted Multiconfiguration-Reference Configuration Interaction Method. *J. Chem. Phys.* **1988**, *89*, 5803-5814.

(27) Knowles, P. J.; Werner, H.-J. Internally Contracted Multiconfiguration-Reference Configuration Interaction Calculations for Excited States. *Theor. Chim. Acta* **1992**, *84*, 95-103.

(28) Werner, H.-J.; Knowles, P. J. A Second Order Multiconfiguration SCF Procedure with Optimum Convergence. *J. Chem. Phys.* **1985**, *82*, 5053-5063.

(29) Tully, J. C. Molecular Dynamics with Electronic Transitions. *J. Chem. Phys.* **1990**, *93*, 1061-1071.

(30) Scholten, M. Semiempirische Verfahren mit Orthogonalisierungskorrekturen: Die OM3 Methode, *Ph.D. thesis*, Universität Düsseldorf, **2003**.

(31) Koslowski, A.; Beck, M. E.; Thiel, W. Implementation of a General Multireference Configuration Interaction Procedure with Analytic Gradients in a Semiempirical Context Using the Graphical Unitary Group Approach. *J. Comput. Chem.* **2003**, *24*, 714-726.

(32) Patchkovskii, S.; Koslowski, A.; Thiel, W. Generic Implementation of Semi-Analytical CI Gradients for NDDO-Type Methods. *Theor. Chem. Acc.* **2005**, *114*, 84-89.

(33) Thiel, W. *MNDO Programm*, Max-Planck-Institut für Kohleforschung: Mühlheim, Germany, 2007.

(34) Swope, W. C.; Andersen, H. C.; Berens, P. H.; Wilson, K. R. A Computer Simulation Method for the Calculation of Equilibrium Constants for the Formation of Physical Clusters of Molecules: Application to Small Water Clusters. *J. Chem. Phys.* **1982**, *76*, 637-649.

(35) El-Sayed, M. A. Triplet State. Its Radiative and Nonradiative Properties. *Acc. Chem. Res.* **1968**, *1*, 8-16.

(36) Bigotto, A.; Galasso, V.; Distefano, G.; Modelli, A. Photoelectron and Electronic Spectra of Acenaphthenequinone, Naphthalic Anhydride, and Naphthalimide. *J. Chem. Soc., Perkin Trans. 2* **1979**, 1502-1506.

(37) Bixon, M.; Jortner, J. Intramolecular Radiationless Transitions. *J. Chem. Phys.* **1968**, *48*, 715-726.

(38) Spighi, G.; Gaveau, M.-A.; Mestdagh, J.-M.; Poisson, L.; Soep, B. Gas Phase Dynamics of Triplet Formation in Benzophenone. *Phys. Chem. Chem. Phys.* **2014**, *16*, 9610-9618.

TOC Figure

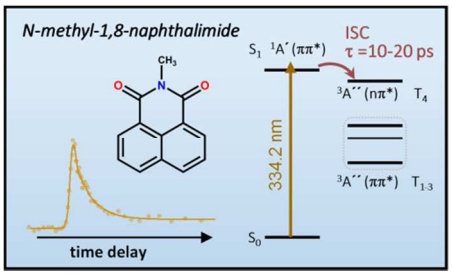

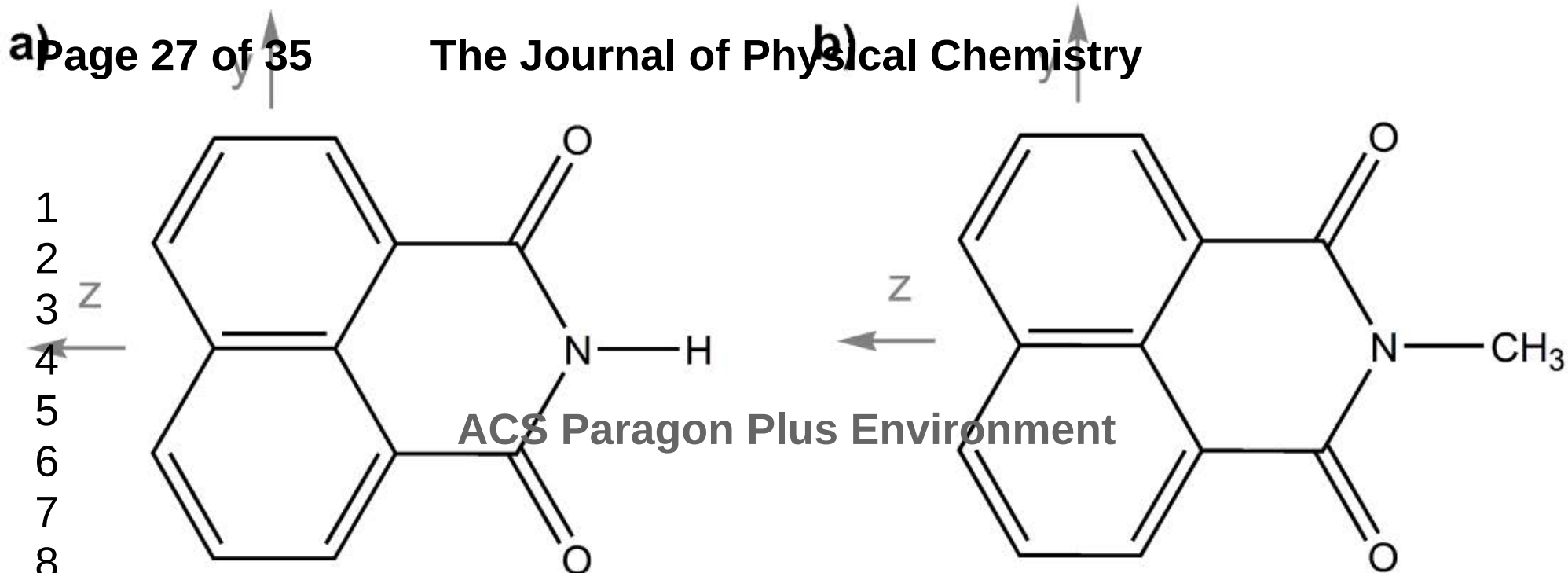

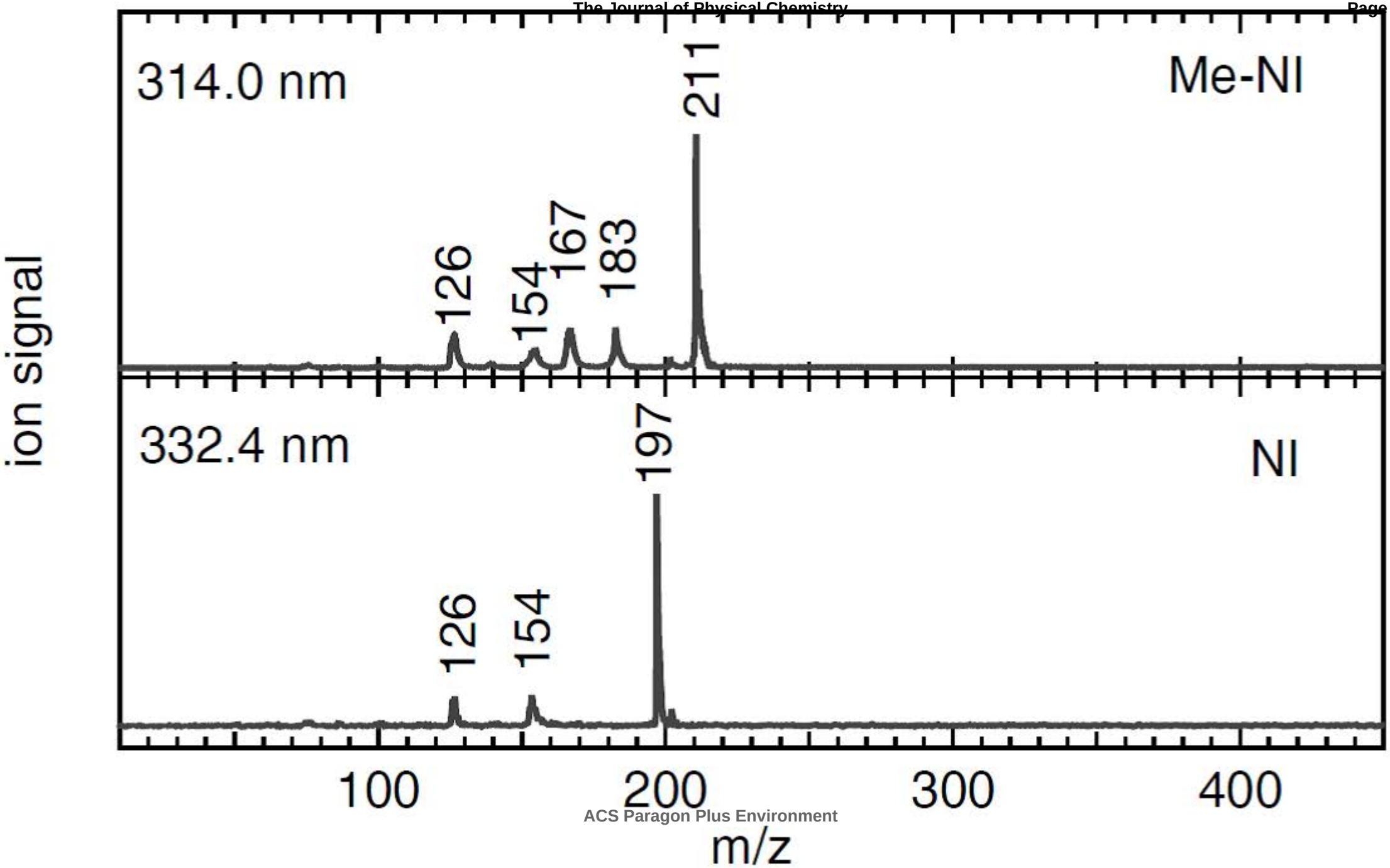
314.0 nm
Me-NI
211
126
154
167
183
332.4 nm
NI
197
126
154
ion signal
100
200
300
400
m/z

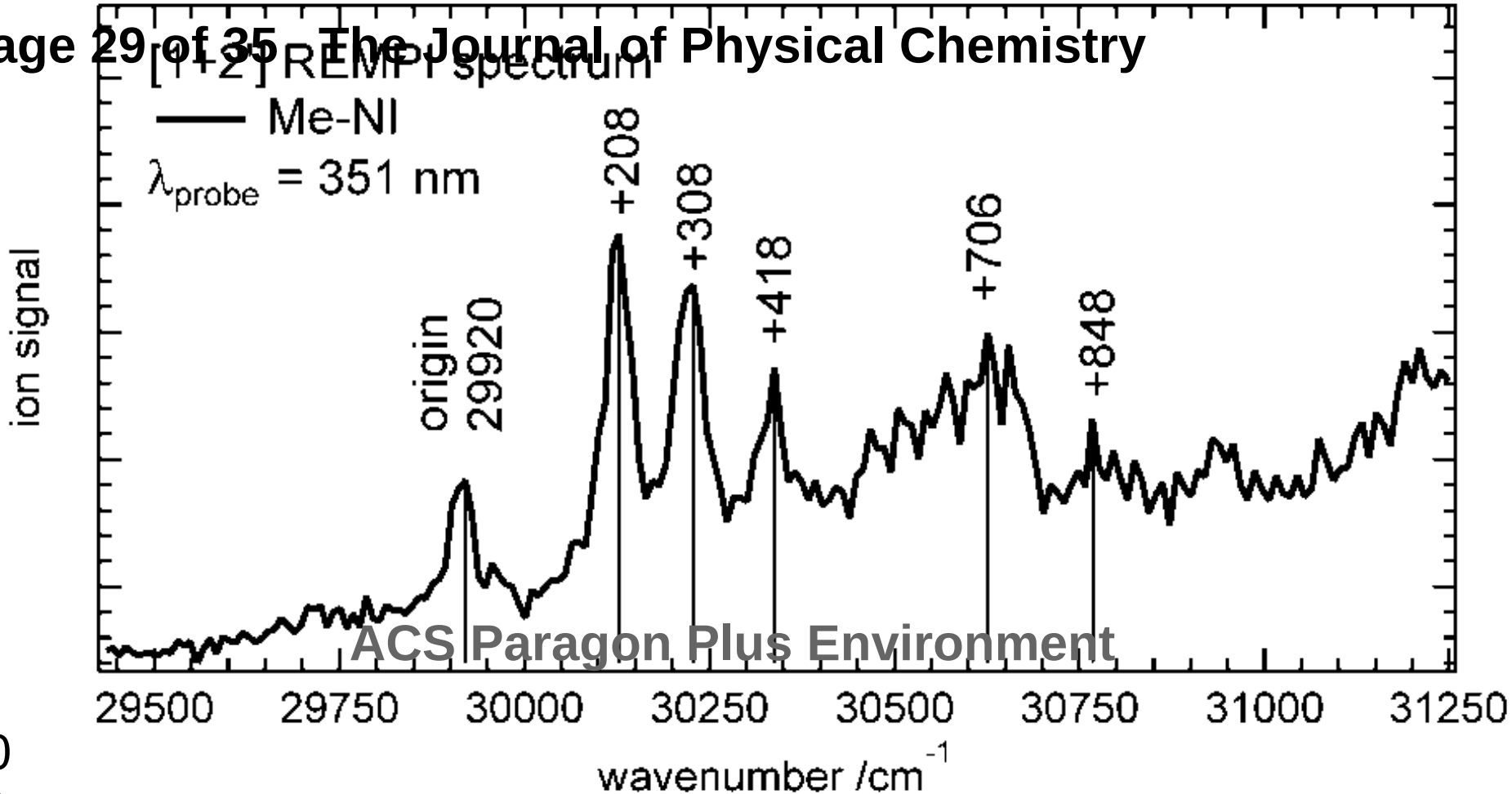

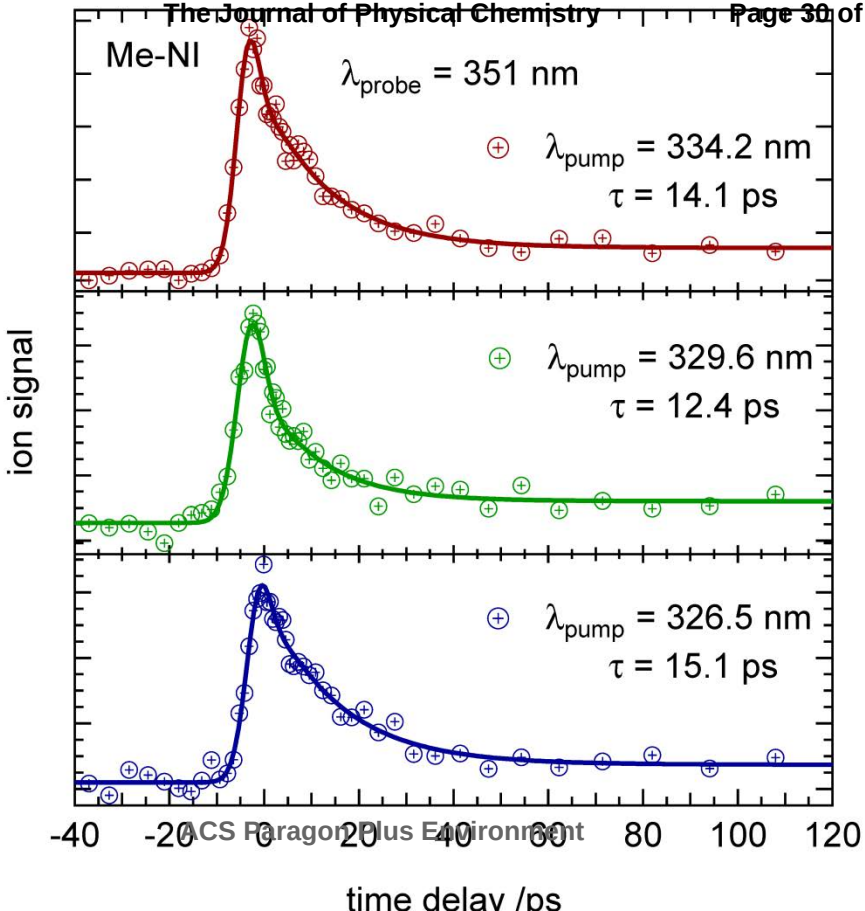

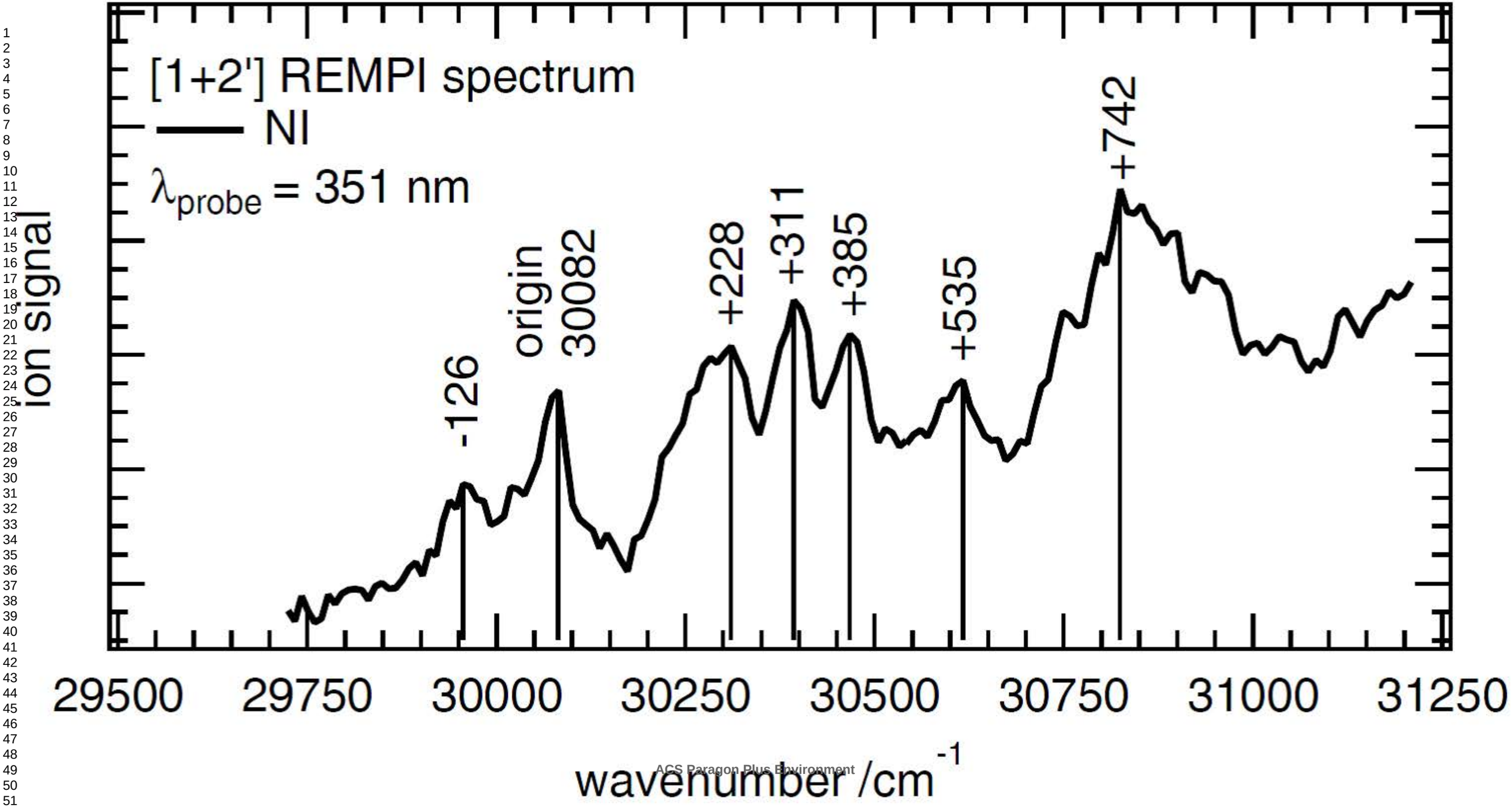
[1+2'] REMPI spectrum
NI
λprobe = 351 nm
ion signal
-126
origin
30082
+228
+311
+385
+535
+742
29500
29750
30000
30250
30500
30750
31000
31250
wavenumber /cm-1

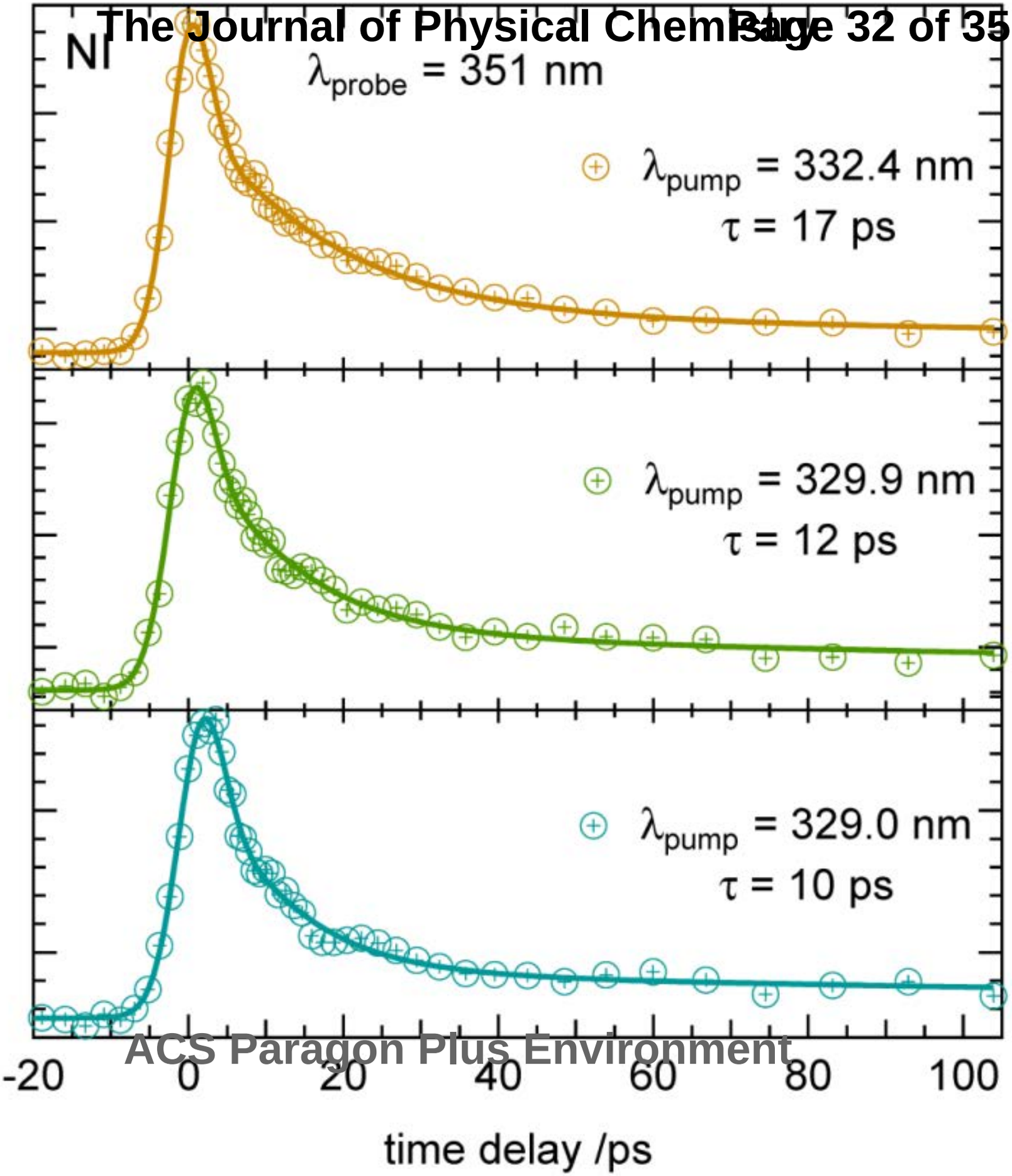
NI
λ_{probe} = 351 nm
λ_{pump} = 332.4 nm
τ = 17 ps
λ_{pump} = 329.9 nm
τ = 12 ps
λ_{pump} = 329.0 nm
τ = 10 ps
ion signal
-20
0
20
40
60
80
100
time delay /ps

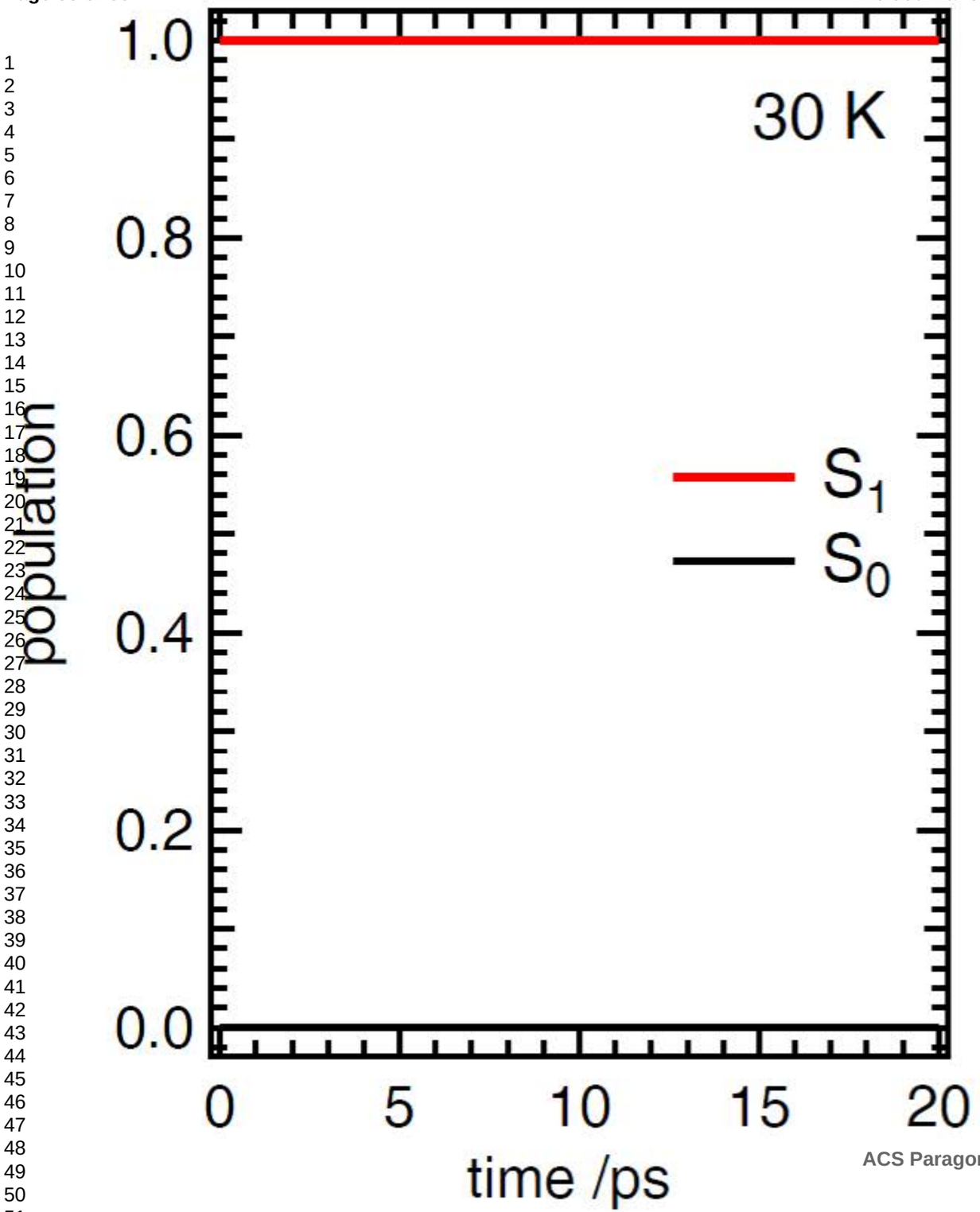
30 K
population
time /ps
S_1
S_0
1.0
0.8
0.6
0.4
0.2
0.0
0
5
10
15
20

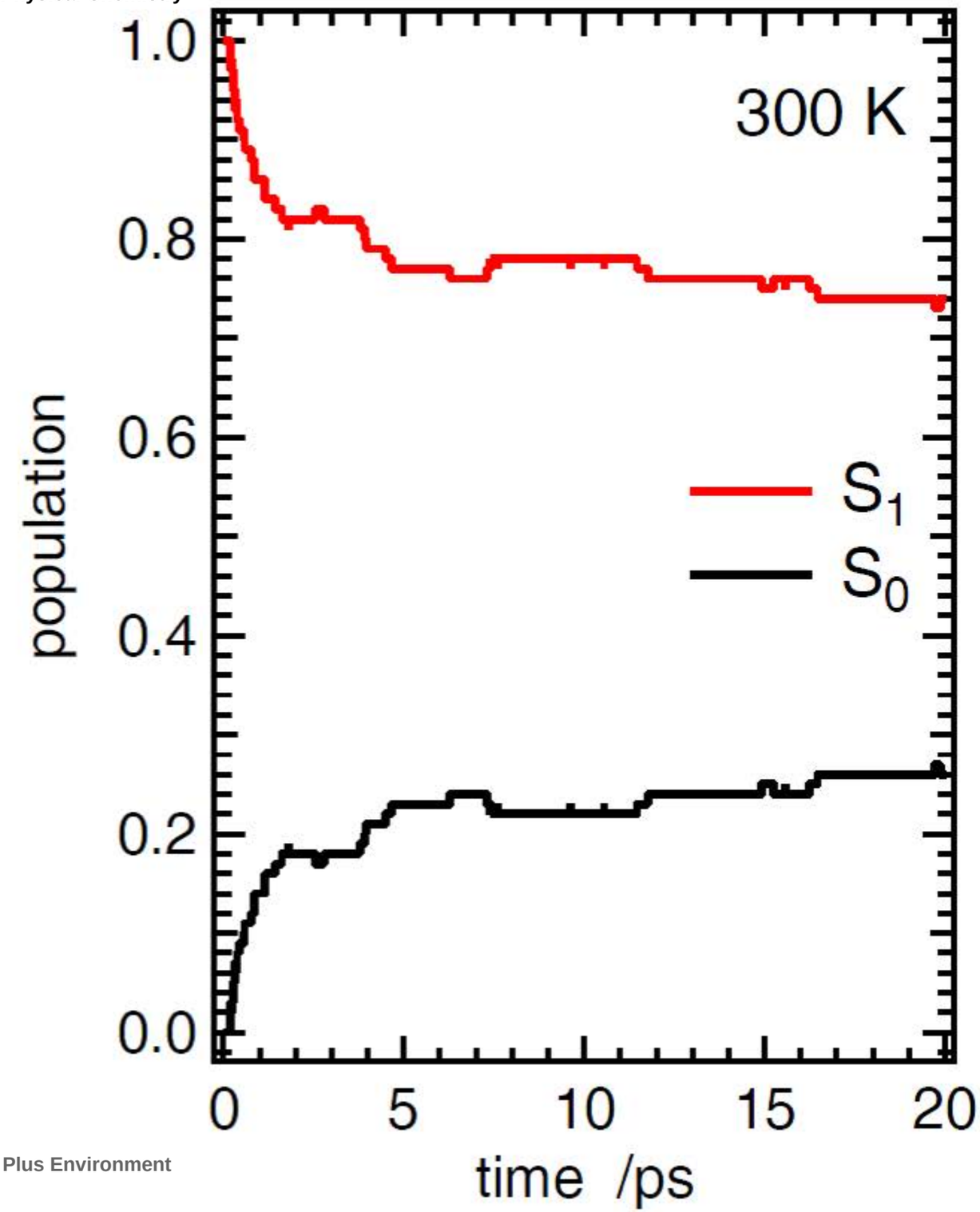
300 K
population
time /ps
S_1
S_0
1.0
0.8
0.6
0.4
0.2
0.0
0
5
10
15
20

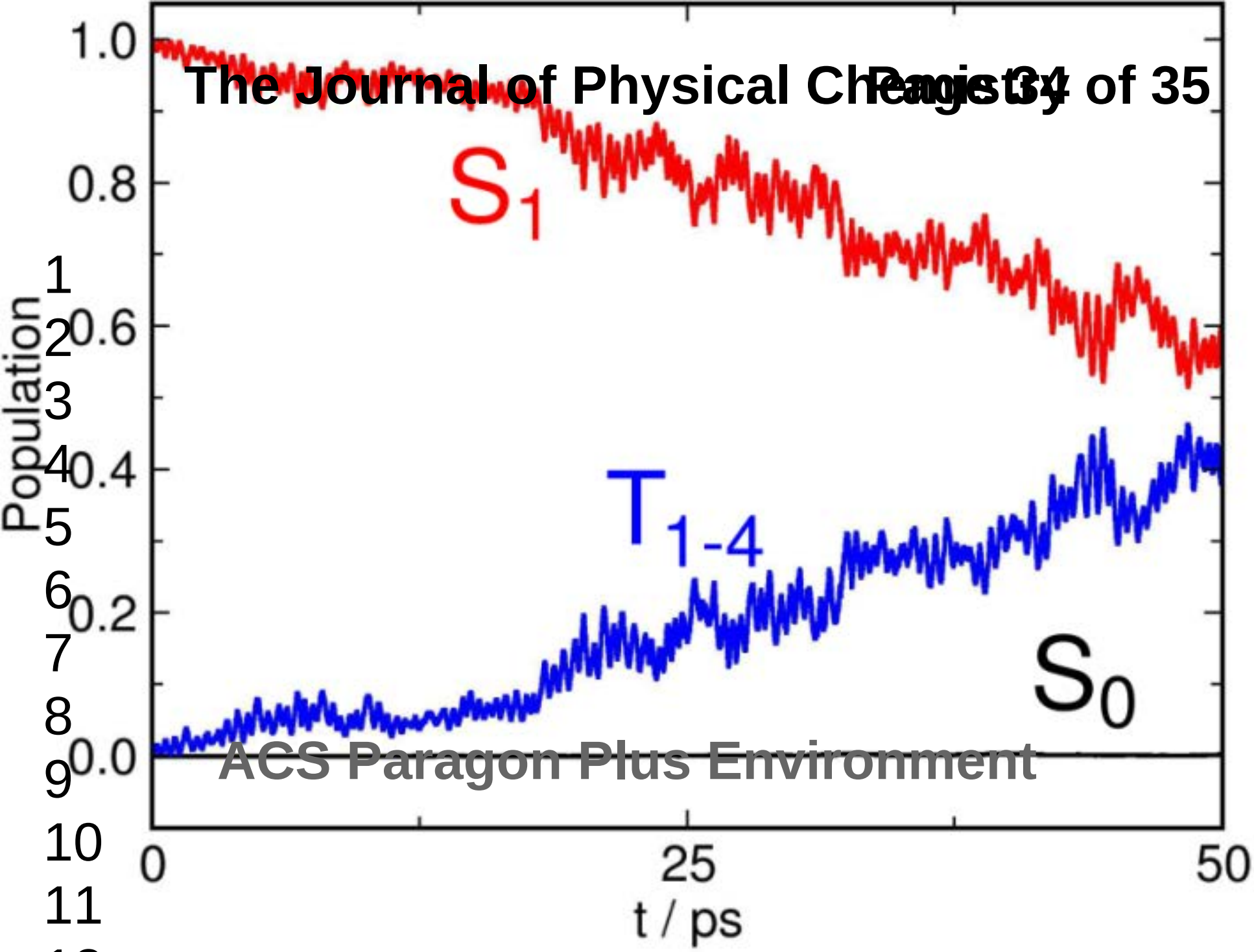

N-methyl-1,8-naphthalimide